Neuro-Oncology 13(9):1037–1046, 2011.
doi:10.1093/neuonc/nor075
Advance Access publication July 29, 2011

Differentiating treatment-induced necrosis from recurrent/progressive brain tumor using nonmodel-based semiquantitative indices derived from dynamic contrast-enhanced T1-weighted MR perfusion

Jayant Narang, Rajan Jain, Ali Syed Arbab, Tom Mikkelsen, Lisa Scarpace, Mark L. Rosenblum, David Hearshen, and Abbas Babajani-Feremi

Division of Neuroradiology, Department of Radiology (J.N., R.J., A.S.A., D.H.); Department of Neurosurgery (R.J., T.M., L.S., M.L.R.); Image Analysis Lab., Radiology Department, Henry Ford Health System, Detroit, MI, USA (A.B.-F.)

Differentiating treatment-induced necrosis (TIN) from recurrent/progressive tumor (RPT) in brain tumor patients using conventional morphologic imaging features is a very challenging task. Functional imaging techniques also offer moderate success due to the complexity of the tissue microenvironment and the inherent limitation of the various modalities and techniques. The purpose of this retrospective study was to assess the utility of nonmodel-based semiquantitative indices derived from dynamic contrast-enhanced T1-weighted MR perfusion (DCET1MRP) in differentiating TIN from RPT. Twenty-nine patients with previously treated brain tumors who showed recurrent or progressive enhancing lesion on follow-up MRI underwent DCET1MRP. Another 8 patients with treatment-naive high-grade gliomas who also underwent DCET1MRP were included as the control group. Semiquantitative indices derived from DCET1MRP included maximum slope of enhancement in initial vascular phase (MSIVP), normalized MSIVP (nMSIVP), normalized slope of delayed equilibrium phase (nSDEP), and initial area under the time-intensity curve (IAUC) at 60 and 120 s ($IAUC_{60}$ and $IAUC_{120}$) obtained from the enhancement curve. There was a statistically significant difference between the 2 groups ($P < .01$), with the RPT group showing higher MSIVP (15.78 vs 8.06), nMSIVP (0.046 vs 0.028), $nIAUC_{60}$ (33.07 vs 6.44), and $nIAUC_{120}$ (80.14 vs 65.55) compared with the TIN group. nSDEP was significantly lower in the RPT group (7.20×10^{-5} vs 15.35×10^{-5}) compared with the TIN group. Analysis of the receiver-operating-characteristic curve showed nMSIVP to be the best single predictor of RPT, with very high (95%) sensitivity and high (78%) specificity. Thus, nonmodel-based semiquantitative indices derived from DCET1MRP that are relatively easy to derive and do not require a complex model-based approach may aid in differentiating RPT from TIN and can be used as robust noninvasive imaging biomarkers.

Keywords: DCE-MRI, MR perfusion, recurrent tumor, semiquantitative indices, treatment-induced necrosis.

Dynamic contrast-enhanced T1-weighted MR perfusion (DCET1MRP) is being increasingly used in various clinical trials involving brain tumors. It allows characterization of the vascular microenvironment in tumors by measurement of a range of parameters, such as K_{trans} (influx transfer constant), K_b (reverse transfer constant), V_e (volume of the extravascular extracellular space), and V_P (blood plasma volume),[1–3] that reflect specific physiologic characteristics and relate to various aspects of tumor biology. However, the biggest hurdle in obtaining these pharmacokinetic quantitative metrics is the use of complicated multicompartment physiologic models to derive these metrics. On the contrary, various nonmodel-based

Received December 10, 2010; accepted April 20, 2011.

Corresponding Author: Rajan Jain, MD, Division of Neuroradiology, Departments of Radiology and Neurosurgery, Henry Ford Health System, 2799 West Grand Blvd. Detroit, MI 48202, USA (rajanj@rad.hfh.edu).

semiquantitative indices are derived from dynamic data, which do not have much physiologic specificity but have been successfully used in the past for evaluation of prostate, breast, cervical, and pancreatic cancers.[4–11] These model-free metrics could have a more practical role to play in the routine clinical setting as well as in multicenter clinical trials, as these do not depend upon technical expertise needed for the more complex model-based analysis. There have also been successful applications of simply applying "curve-ology" to DCE-MRI time courses,[12] i.e., merely considering the shape of the uptake and washout of the contrast agent.[13,14] This approach has been particularly successful in breast cancer imaging.[7] However, these semiquantitative indices have not been used much in the evaluation of brain tumors.

Differentiating treatment-induced necrosis (TIN) from recurrent/progressive tumor (RPT) is a common yet challenging task in a busy neuro-oncologic practice. The importance of differentiating these 2 entities cannot be overemphasized, as the treatment options and prognosis for the 2 are different. With the advent of newer aggressive treatment options for brain tumors, including various combination neoadjuvant therapeutic strategies, the follow-up imaging appearance of a previously treated brain tumor is also becoming more and more complex. There have been various attempts to differentiate these 2 entities in the past using conventional morphologic imaging[15–17] as well as various functional imaging techniques such as CT perfusion,[18,19] MR perfusion,[20,21] diffusion weighted imaging,[22,23] MR spectroscopy,[24–27] and single-photon emission computed tomography and PET.[28,29] However, each modality has its limitations, and the search for an easy to use yet accurate modality continues.

The purpose of this retrospective study is to show the utility of nonmodel-based DCET1MRP semiquantitative indices as simple to derive yet robust imaging biomarkers that can be used to differentiate RPT from TIN.

Materials and Methods

Study Group

This retrospective study is compliant with the Health Insurance Portability and Accountability Act and was approved by our institutional review board. Twenty-nine patients with previously treated brain tumors who showed recurrent or progressive enhancing lesions on follow-up MR imaging and underwent DCET1MRP were included in this study. Another 8 patients with treatment-naive high-grade gliomas who underwent DCET1MRP were included as the control group. Twenty of the 29 patients were diagnosed with RPT, and 9 patients with TIN. Fifteen (75%) cases of RPT and 5 (55.5%) of TIN underwent surgery and histological confirmation. For the patients who did not undergo histological confirmation, a diagnosis of RPT or TIN was reached on the basis of imaging and clinical follow-up (3–13 months follow-up with stable or reduced size of the lesion without any change in treatment in the TIN group versus further imaging and clinical progression in the RPT group).

DCET1MRP Technique and Semiquantitative Indices

DCET1MRP was performed on a 3-Tesla clinical MR system (Excite HD, GE Medical Systems). A dynamic 3D spoiled gradient echo series was obtained during and after injection of a gadolinium (Gd)-based contrast agent (0.1 mmol/kg) via a power injector (3 mL/s), followed by a flush of 20 mL of normal saline at the same rate. Multiphase acquisition was used with each phase acquired in 5.5 s, and injection started after 6 baseline phases (total imaging time: 6 min 16 s; 70 phases; slice thickness: 5 mm with no gap; TR 5–6 ms, echo time (TE) = 0.75 ms, and field of view (FOV) = 24 cm).

Contrast agents such as Gd-DTPA selectively alter the T1-weighted MRI signal intensity (SI) through their effects on relaxation rates of water in tissues.[30] After a bolus i.v. injection, Gd-DTPA is rapidly distributed throughout the blood plasma, extravasates into the interstitial space (initial vascular phase), and then diffuses back into the vasculature (washout or delayed equilibrium phase). By applying DCE-MRI, it is possible to measure the SI of a region of interest (ROI) before the arrival of a contrast agent (baseline) and to observe the change in SI during the initial vascular phase and the delayed equilibrium phase. This allows the construction of an SI–time curve and the measurement of various dynamic variables of contrast enhancement. Semiquantitative indices were calculated from the SI–time curve using an in-house MATLAB-based software. Extraction of these features is illustrated in Figure 1.

ROIs were drawn manually on the DCET1MRP parametric maps, including only the solid enhancing component of the recurrent lesion. ROIs were drawn on all the axial sections where the recurrent enhancing lesion was present, and then a mean of all sections was obtained. All ROIs were placed to avoid the major vessels and the cystic or necrotic part of the recurrent lesion as much as possible.

Statistical Analysis

All data were expressed as mean ± standard deviation (SD). To assess the significant differences among various semiquantitative indices derived from the RPT group, the TIN group, and controls (treatment-naive high-grade gliomas), an analysis of variance followed by a post-hoc test (Fisher's protected least significant difference) were applied; $P < .05$ was considered significant. Binary logistic regression and analyses of the receiver operating characteristic (ROC) curves were used to assess the diagnostic utility (sensitivity, specificity, and predictive values) of using various indices to discriminate RPT from TIN. Cutoff points were also calculated to differentiate the 2 entities; $P < .05$ was considered statistically significant.

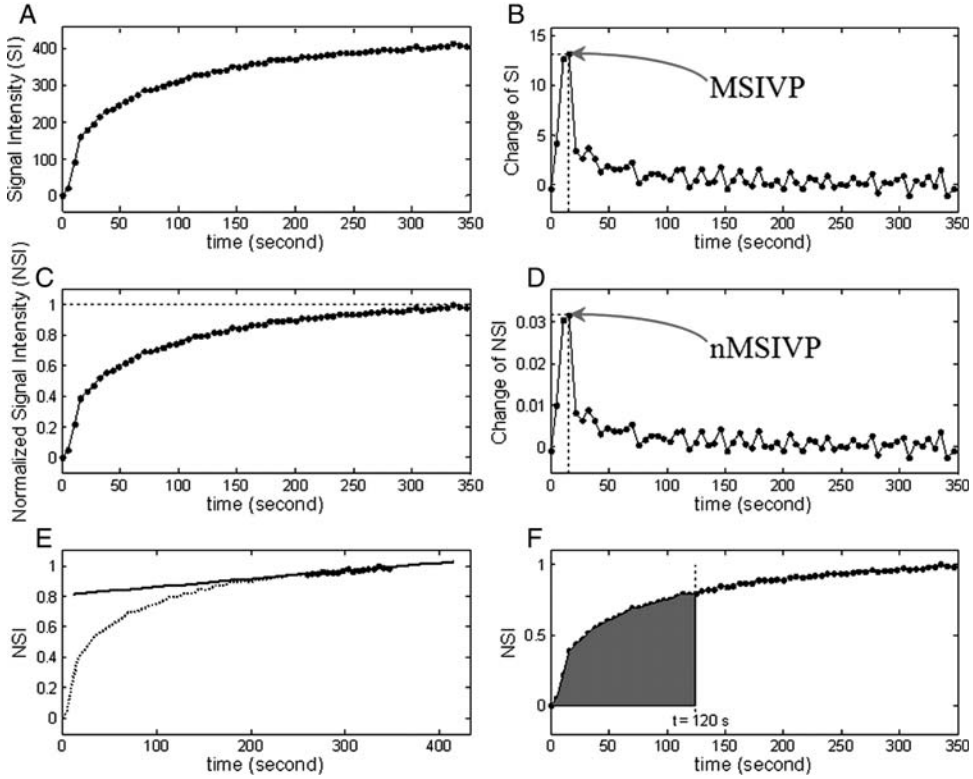

Fig. 1. Calculation of various nonmodel-based indices obtained from the signal intensity (SI)-time curve. (A) Representative SI-time curve of a tumor region of interest. (B) Change of the SI per unit time that the maximum value in this figure represents maximum slope of enhancement in initial vascular phase (MSIVP). (C) Normalized (to peak) SI. (D) Change of the normalized SI per unit time that the maximum value in this figure represents normalized maximum slope of enhancement in initial vascular phase (MSIVP). (E) We performed a linear least square fit to the final 25% of samples of the normalized SI, and we defined the normalized slope of the delayed equilibrium phase (normalized slope of delayed equilibrium phase (nSDEP) as the slope of the fitted line, as shown in Figure 1E). (F) The area under the normalized curve within the time limits 0–120 s represents $nIAUC_{120}$.

Results

Out of 29 patients, 9 were diagnosed with TIN and 20 with RPT (Table 1). Twenty-four patients underwent treatment for a primary brain neoplasm (WHO grade II = 1, grade III = 5, grade IV = 17; hemangiopericytoma $n = 1$), and 5 patients had metastatic disease (brain metastases from lung carcinoma $n = 2$, ovarian carcinoma $n = 1$, breast carcinoma $n = 1$, and thyroid carcinoma $n = 1$). Twenty-seven patients underwent surgery (subtotal resection $n = 18$, gross total resection $n = 8$, and biopsy $n = 1$) for the primary lesion, and 2 patients did not have any surgery. All patients underwent radiation therapy, whereas only 25 patients received adjuvant chemotherapy as well (external-beam radiation therapy, 55–60 Gy, $n = 23$; stereotactic radiosurgery, 14–16 Gy, $n = 5$; intensity-modulated radiation therapy, 59.4 Gy, $n = 1$). Time intervals between the appearance of the recurrent/progressive enhancing lesion and radiation therapy were as follows: for the RPT group, 2–68 months (mean, 12 months); for the TIN group, 4.4–14.0 months (mean, 7.8 months) (Table 1).

Analysis for the Whole Group

All the indices showed statistically significant differences between the RPT and TIN groups ($P < .01$) (Fig. 2 and Table 2), with the RPT group showing a higher maximum slope of enhancement in the initial vascular phase (MSIVP; 15.78 vs 8.06), a higher normalized MSIVP (0.046 vs 0.028), and a higher initial area under the time-intensity curve at 60 s ($IAUC_{60}$; 33.07 vs 25.45) and at 120 s ($IAUC_{120}$; 80.14 vs 65.55), while the normalized slope of the delayed equilibrium phase (nSDEP) was lower (7.20×10^{-5} vs 15.35×10^{-5}) compared with the TIN group. The control group (treatment-naive high-grade gliomas) also showed statistically significant differences ($P < .05$) compared with the RPT and TIN groups, except for MSIVP, which was significantly different between the TIN and control groups but not between the control and RPT groups. Mean values of normalized (n)MSIVP (0.067), $nIAUC_{60}$ (43.34), and $nIAUC_{120}$ (95.52) were higher in the control group compared with both RPT and TIN groups. Similarly, the mean value of nSDEP (3.05×10^{-5}) was lower in the control group compared with both RPT and TIN groups.

Table 1. Patient Demographics

	TIN ($n = 9$)	RPT ($n = 20$)
Age, years (range)	51.4 (18–70)	52.3 (28–66)
Sex, M:F	4:5	3:2
Primary brain tumor	8	16
WHO grade II	–	1
WHO grade III	–	5
WHO grade IV	7	10
Others	1	0
Metastasis	1	4
First surgery for primary tumor		
Biopsy	0	1
Subtotal resection	6	12
Gross total resection	2	6
Adjuvant therapy		
Radiation and chemotherapy	8	17
Only radiotherapy	1	3
Time interval between radiotherapy and appearance of recurrent/progressive lesion (months)	4–14	2–68
Patients on steroids at the time of DCET1MRP examination	1	5

TIN, treatment-induced necrosis; RPT, recurrent/progressive tumor; DCET1MRP, dynamic contrast-enhanced T1-weighted MR perfusion.

Binary logistic regression and ROC curve analyses with cutoff points to differentiate RPT from TIN are presented in Figure 3 and Table 3. Table 3 summarizes the stepwise variable selection and selected combinations of sensitivity and specificity achieved (corresponding to points on the ROC curve) when considering different indices. nMSIVP was the best single predictor of RPT, with very high (95%) sensitivity and high (78%) specificity using a cutoff point of 0.031. nSDEP was found to be the most specific predictor of RPT, with a very high specificity (100%) and sensitivity (85%) using a cutoff point of 10.70×10^{-5}. For MSIVP, a cutoff point of 9.94 was found to differentiate RPT from TIN with a sensitivity of 90% and specificity of 100%. For $nIAUC_{60}$, a cutoff point of 27.37 yielded 80% sensitivity and 78% specificity. A sensitivity of 85% and specificity of 78% to differentiate RPT from TIN was found with $nIAUC_{120}$ using a cutoff point of 73.85.

ROC-AUC analysis (Fig. 3) indicated that the diagnostic models based on all the indices considered alone had a statistically significant *P*-value, with AUC $\geq$ 0.90. (MSIVP = 0.94, nMSIVP = 0.93, nSDEP = 0.93, $nIAUC_{60} = 0.90$, and $nIAUC_{120} = 0.90$). MSIVP did the best, with AUC of 0.94, followed by nMSIVP and nSDEP with AUC of 0.93.

Analysis for the High-Grade Glioma Group

A separate analysis of 22 patients (RPT $n = 15$, TIN $n = 7$) who underwent treatment for only high-grade gliomas was also done. In this analysis as well, all the indices showed statistically significant differences between RPT and TIN groups ($P < .01$), with the RPT group showing higher MSIVP (16.46 vs 7.83), nMSIVP (0.046 vs 0.029), $nIAUC_{60}$ (33.45 vs 25.45), and $nIAUC_{120}$ (80.68 vs 64.87), and lower nSDEP (7.03×10^{-5} vs 15.73×10^{-5}) compared with the TIN group. The control group (treatmeny-naive high-grade gliomas) also showed statistically significant differences ($P < .05$) compared with the RPT and TIN groups, except for MSIVP, which was significantly different between the TIN and control groups but not between the control and RPT groups.

ROC-AUC analysis for this subgroup indicated that the diagnostic models based on all the indices considered alone had a statistically significant *P*-value with AUC $\geq$ 0.90 (MSIVP = 1.00, nMSIVP = 0.90, nSDEP = 0.96, $nIAUC_{60} = 0.90$, and $nIAUC_{120} = 0.90$). MSIVP was the best single predictor of RPT, with a sensitivity and specificity of 100% using a cutoff point of 9.5.

Discussion

In this study, various model-free, simple mathematical indices of SI-time curves acquired using DCET1MRP were correlated for the differences in RPT, TIN, and treatment-naive high-grade gliomas. We found that all of these semiquantitative indices were significantly different and hence could be used as imaging biomarkers in differentiating RPT from TIN.

In a treated brain tumor patient with a recurrent or progressive enhancing lesion, it is imperative to differentiate RPT from TIN, as the prognosis and treatment for these entities differ significantly. Both entities often manifest as an enlarging mass with varying degrees of surrounding edema and progressive enhancement on serial MR images, which is usually very difficult to differentiate based on conventional morphologic imaging alone.[15–17] Various metabolic (MR spectroscopy and PET) and physiologic (diffusion-weighted,

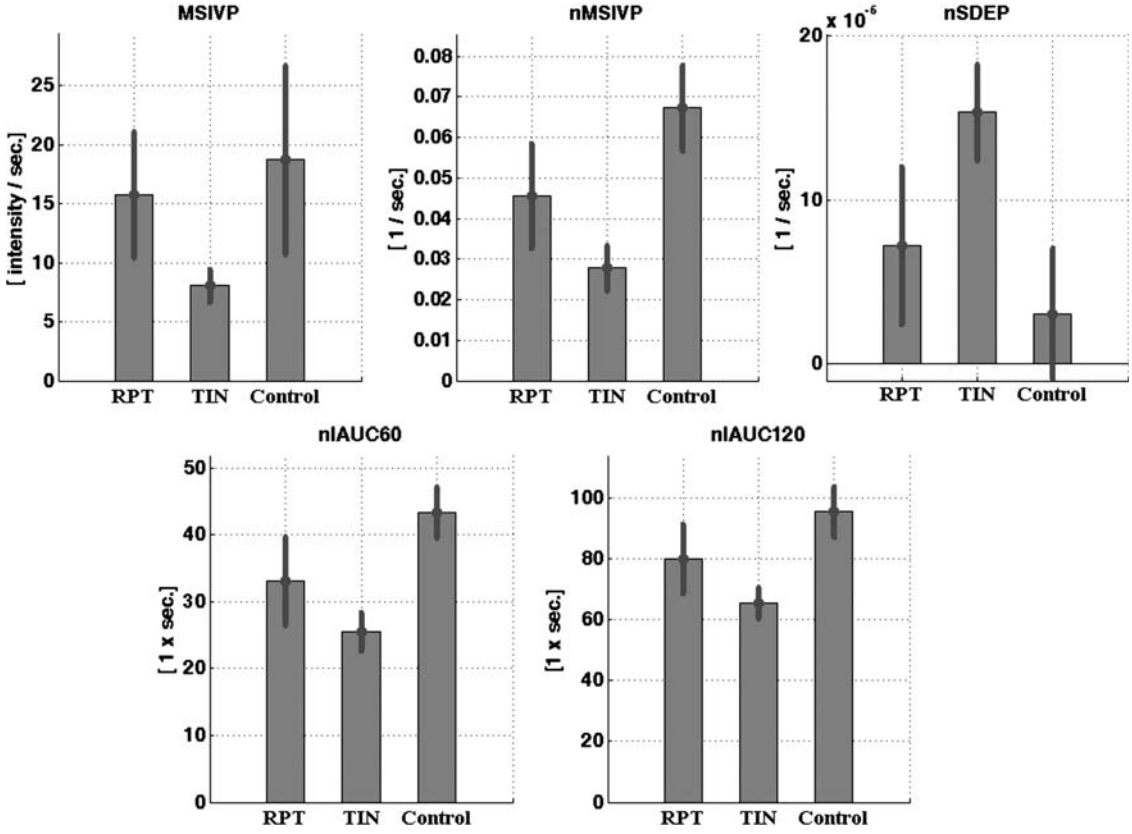

Fig. 2. Plot of mean and standard deviation showing various nonmodel-based semiquantitative indices derived from dynamic contrast-enhanced T1-weighted MR perfusion (DCET1MRP) in treatment-induced necrosis (TIN) and recurrent/progressive tumor (RPT) groups.

Table 2. Descriptive Statistics (mean and SD) of Various Nonmodel-based Semiquantitative Indices Derived from DCET1MRP for the Whole Group

	RPT	TIN	*P*-value	Controls	*P*-value	
					vs RPT	vs TIN
MSIVP (Intensity/s)	15.78 ± 5.44	8.06 ± 1.41	.001	18.73 ± 8.52	.220	<.001
nMSIVP (1/s)	0.046 ± 0.013	0.028 ± 0.006	<.001	0.067 ± 0.011	<.001	<.001
nSDEP (1/s)	$7.20^{-5} \pm 4.91^{-5}$	$15.35^{-5} \pm 3.11^{-5}$	<.001	$3.05^{-5} \pm 4.26^{-5}$	.03	<.001
$nIAUC_{60}$ (1 × s)	33.07 ± 6.44	25.45 ± 3.18	.001	43.34 ± 4.04	<.001	<.001
$nIAUC_{120}$ (1 × s)	80.14 ± 11.64	65.55 ± 5.55	<.001	95.52 ± 8.71	<.001	<.001

RPT, recurrent/progressive tumor; TIN, treatment-induced necrosis; MSIVP, maximum slope of enhancement in initial vascular phase; nMSIVP, normalized MSIVP; nSDEP, normalized slope of delayed equilibrium phase; nIAUC, initial area under the time-intensity curve.

diffusion tensor, and perfusion) imaging techniques have been used in the past with variable success.[31] However, most of the clinically available imaging tools suffer from some limitation not just due to the limited resolution but also due to the complexity of the tissue microenvironment. This is further complicated by the fact that most of these recurrent or progressive enhancing lesions are mixtures of variable degrees of tumor and treatment effects and rarely have either pure tumor or necrosis. CT perfusion has been used with good success,[18,19] particularly due to the fact that there is a linear relationship between tissue attenuation and contrast agent concentration, which makes the postprocessing less prone to assumptions, and CT perfusion has an arterial input function, unlike MR perfusion techniques. However, its utilization is limited due to concerns for radiation exposure as well as its need for a separate examination, whereas MR perfusion can be done as part of the standard of care follow-up MRI without needing additional contrast injection. Dynamic susceptibility contrast-enhanced MR perfusion has also been successfully used in the past,[20,21,32] but apart from the above described limitations of any MR perfusion technique, it also suffers from susceptibility artifacts,

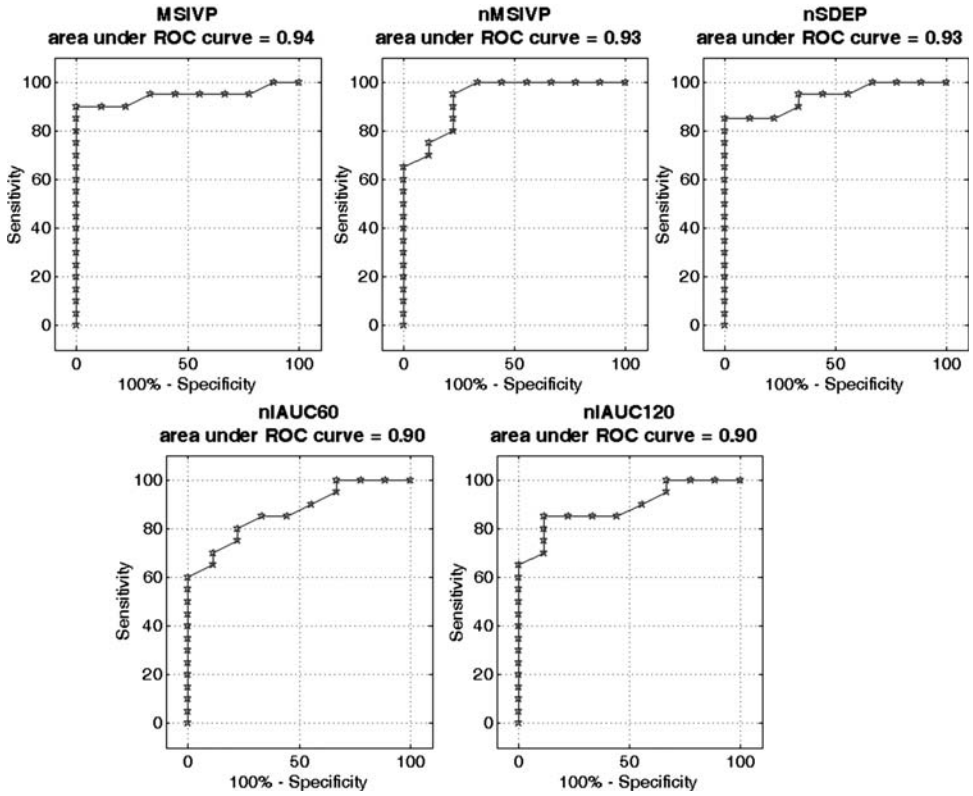

Fig. 3. Receiver operating characteristic (ROC) curves associated with the model to differentiate recurrent/progressive tumor (RPT) from treatment-induced necrosis (TIN) using various nonmodel-based semiquantitative indices derived from dynamic contrast-enhanced T1-weighted MR perfusion (DCET1MRP) considered individually. All these curves have AUC of $\geq$0.90, which is considered to be statistically significant. MSIVP, maximum slope of enhancement in initial vascular phase; nMSIVP, normalized MSIVP; nSDEP, normalized slope of delayed equilibrium phase; nIAUC, initial area under the time-intensity curve.

Table 3. Selected Combinations of Sensitivity and Specificity Achieved (corresponding to points on the ROC curve in Figure 3) for Differentiating RPT and TIN When Considering Different Indices Individually

MSIVP			nMSIVP			nSDEP		
Sensitivity	Specificity	Cutoff Value	Sensitivity	Specificity	Cutoff Value	Sensitivity	Specificity	Cutoff Value
100	11	6.43	100	67	0.029	100	35	17.57×10^{-5}
95	67	8.14	95	78	0.031	95	67	13.7×10^{-5}
90	100	9.94	75	89	0.035	85	89	12.0×10^{-5}
			65	100	0.037	85	100	10.70×10^{-5}
$nIAUC_{60}$			**$nIAUC_{120}$**					
Sensitivity	Specificity	Cutoff Value	Sensitivity	Specificity	Cutoff Value			
100	33	23.25	100	33	62.46			
85	67	26.33	85	78	68.85			
80	78	27.37	70	89	73.85			
60	100	30.18	65	100	74.00			

MSIVP, maximum slope of enhancement in initial vascular phase; nMSIVP, normalized MSIVP; nSDEP, normalized slope of delayed equilibrium phase; nIAUC, initial area under the time-intensity curve.

which could be a slightly bigger issue in previously treated patients due to the presence of hemorrhage, calcification, and surgical clips.

DCET1MRP could be a promising diagnostic tool in the differentiation of RPT from TIN, as it is much less susceptible to artifacts and allows accurate characterization of the vascular microenvironment of the lesion. However, it has the disadvantage of complexity of quantification of various perfusion parameters because of a nonlinear relationship between SI and contrast agent concentration as well as requirement of complex multicompartment physiological models to

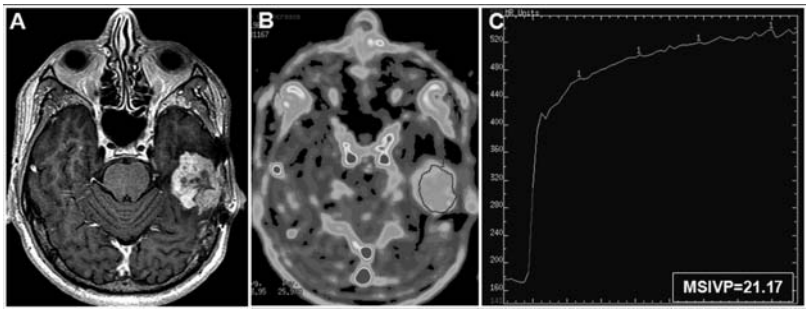

Fig. 4. A 40-year-old male with initial diagnosis of WHO grade III astrocytoma underwent gross total resection and received chemotherapy and external-beam radiotherapy (54 Gy). (A) Follow-up MRI showed appearance of a recurrent enhancing lesion 19 months postradiotherapy in the right temporal region within the radiation field. (B) maximum slope of enhancement in initial vascular phase (MSIVP) parametric map and (C) graph of MSIVP showed high MSIVP, suggesting recurrent/progressive tumor (RPT), which was confirmed by histopathology.

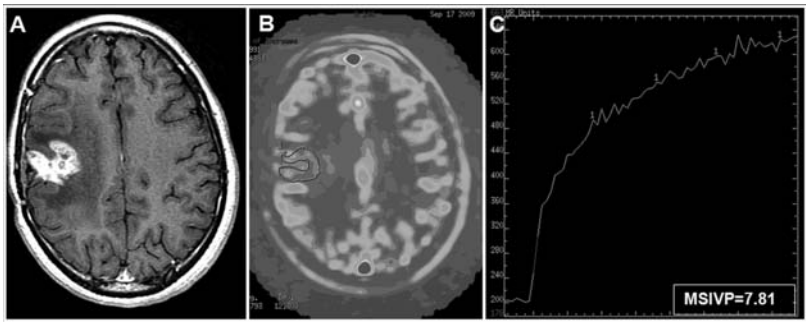

Fig. 5. A 19-year-old female with initial diagnosis of glioblastoma multiforme received chemotherapy and external beam radiotherapy (60 Gy). (A) Twelve months postradiotherapy, follow-up MRI showed development of a recurrent enhancing lesion in left parietal region. (B) Maximum slope of enhancement in initial vascular phase (MSIVP) parametric map and (C) graph of MSIVP showed low MSIVP, suggesting treatment-induced necrosis, which was confirmed by histopathology.

derive pharmacokinetic values. It also involves calculation of baseline T1 values and an arterial input function, which are prone to errors.[2,33–36] Because of these reasons, a robust and yet user-friendly software to process DCET1MRP data is far from lacking in today's clinical practice. In an attempt to obviate the need for such software and complex postprocessing, we propose the use of simple to derive yet robust semiquantitative indices derived from DCET1MRP. These indices may be more suitable for use within a clinical setting because they are less reliant on the technical expertise required for more complex analysis processes and can be obtained fairly quickly. Many of these qualitative and semiquantitative measurements have been used in the past in evaluating prostate cancer,[4,5,8] breast cancer,[6,7,7,13,14] pancreatic cancer,[11] and cervical cancer.[9,10]

DCET1MRP Derived Semiquantitative Indices

The term "semiquantitative" can be misleading, as semiquantitative parameters, though lacking clear physiologic understanding, can be fully quantitative in that these can be measured objectively and reproducibly. Nonmodel-based methods have the obvious advantage of being very straightforward to implement and can be performed in near real time. Their obvious limitations include the fact that these semiquantitative parameters do not necessarily have clear physiologic correlates, since they are "mixed" measures of tissue blood flow and vascular permeability as well as an indirect measure of the extravascular extracellular space (EES). Additionally, the degree to which each of these physiologic parameters contributes to the time enhancement curve is at least partially determined by an arbitrarily selected time point as the end of the initial portion of the enhancement curve; in this light, they are not pure measures of "physiology." It should also be noted that since these methods rely on SI measurements (and not a physical measurement like *T1*), it may be inherently difficult to compare scans performed at separate times. For this same reason, semiquantitative methods may also be difficult to compare among institutions.[12]

Generally, tissue enhancement following contrast medium administration is dependent on various physiologic factors, including tissue vascular density and surface area, vascular permeability, blood flow, and composition of the EES, as well as interstitial pressure. However, the degree of tissue enhancement also varies over time due to the complex interaction of these factors, which is based on the tissue composition that

will be different for RPT and for TIN. One of the indices used for the present study included estimation of MSIVP and nMSIVP. Both were significantly higher in the RPT group (Fig. 4) compared with the TIN group (Fig. 5). This initial slope probably reflects early enhancement due to the early vascular phase, which derives mostly from the contrast agent in the blood vessels, and hence tissue vascular density, but also from the early leakage of contrast agent into the EES due to a deficient blood-brain barrier. However, this component of early permeability in the initial vascular phase is dependent mostly upon the blood flow as well as total vascular surface area exposed to the contrast agent. RPTs are usually higher grade tumors with increased vascularity due to neoangiogenesis (or increased microvascular density) compared with TINs, which show hyalinized vasculopathy and coagulative necrosis leading to hypoperfusion. Therefore, RPTs have a higher MSIVP and nMSIVP due to a prominent early vascular phase based on hypervascularity and neoangiogenesis.

Delayed imaging obtained after the initial vascular phase (or the first pass) is optimal to evaluate the washout or the equilibrium phase of contrast agent and may also be helpful to differentiate RPT from TIN. This phase probably includes mostly delayed permeability and slow accumulation of contrast agent into the EES, the majority of which is dependent on the backflow of contrast agent into the intravascular compartment, which in turn depends upon V_e and interstitial pressure as well as total vascular area or density available to the contrast agent. In the present study, nSDEP, a measure of SI change in the washout or equilibrium phase, was significantly higher in TIN than in RPT, as determined by the positive final slope (15.35×10^{-5} vs 7.20×10^{-5}). This could be explained by increased V_e in TIN due to less cellularity and more tissue damage, leading to more retention of contrast agent in the EES, less backflow, and reduced washout with higher nSDEP. On the contrary, RPT will have higher cellularity and lower V_e in addition to higher interstitial pressure due to tumor growth and angiogenesis, both of which will reduce retention of contrast agent in the EES, increase the backflow and washout and hence lower nSDEP. Lee et al.[37] showed that there was a decrease in the percentage signal recovery (PSR) with increase in the radiation dose in the irradiated normal brain, which they attributed in part to accumulation of contrast in the EES due to elevated microvascular permeability. However, we think that PSR is dependent not just upon permeability but also on V_e, which will be increased with radiation injury, causing tissue damage and lower cellularity.

IAUC has been used in the past and shown to be a simple, reliable, and reproducible metric; however, the physiological meaning of the IAUC has not been rigorously defined with respect to model-based parameters.[38–41] Previous authors[38] have shown that IAUC is a mixed parameter that can display correlation with K_{trans}, V_e, and V_p and ultimately has an intractable relationship with all three, although these authors used a concentration-time curve and we used an SI-time curve to derive the IAUC. In our study, $IAUC_{60}$ and $IAUC_{120}$ were both significantly different among the TIN, RPT, and control groups.

There has been an attempt to compare model- and nonmodel-based methods of DCE-MRI in the literature.[40] Roberts et al.[40] concluded that although modeling is more complex than the nonmodel-based approach, the former is preferable as it provides greater physiologic insight. However, in the present study, we have tried to emphasize the utility of these nonmodel-based approaches in routine clinical practice where easy to derive parameters could be more practical. Our results are consistent with those of Hazle et al.,[42] who used Max dI/dt (similar to MSIVP of the present study) to successfully differentiate RPT and TIN. Zelhof et al.[4] also used various semiquantitative variables to differentiate prostate cancer and normal peripheral zone regions. Zahra et al.[10] showed that both quantitiative and semiquantitative indices were useful in predicting radiation response in carcinoma cervix patients.

Our study had several limitations, including its retrospective nature and the small sample size, particularly of histopathology proven radiation necrosis cases. Another important limitation is that 5 (25%) RPT patients were on a stable dose of steroids at the time of DEC-MRI examination compared with only 1 (11%) of the TIN patients, which would repair the damaged blood-brain barrier and could potentially affect the results. We included patients with gliomas as well as metastases in the present analysis, which could be a potential limitation of the study; however, we also did a separate analysis for the high-grade glioma group, which revealed similar results, and in fact MSIVP showed a sensitivity and specificity of 100% for differentiating RPT and TIN in the high-grade glioma group. A review of the literature also suggests that there are no significant differences in the blood volume estimates of enhancing portion of high-grade gliomas and metastases,[43] although there are significant differences in perfusion characteristics in the peritumoral region because of peritumoral infiltration by high-grade gliomas.[43] Cha et al. also showed PSR to be different in glioblastomas and metastases.[43] However, when differentiating recurrent metastases or recurrent glioma from radiation necrosis, both showed significantly higher perfusion values than necrosis.[18,21,44–46]

Conclusions

DCET1MRP is being more commonly used in multicenter brain tumor clinical trials, as there is increasing emphasis on using quantitative imaging biomarkers particularly with the newer anti-angiogenic agents. However, its practical impact on routine neuro-oncologic imaging practice is restricted by the need for complicated multicompartment physiologic models and intensive computational requirements to derive pharmacokinetic metrics and the lack of an easy

to use and yet robust commercially available software. We propose the use of nonmodel-based semiquantitative indices derived from DCET1MRP in differentiating RPT from TIN that are relatively easy to derive, are robust, are reproducible, and do not require a complicated model-based approach for calculation. These indices, though they may not have a specific physiologic basis, may still serve the purpose of a robust and easy to use clinical tool that can help in quick and efficient decision making.

Acknowledgments

We would like to thank Ms. Nandita Mani for help with manuscript preparation.

Funding

None.

Conflict of interest statement. None declared.

References

1. O'Connor JP, Jackson A, Parker GJ, et al. DCE-MRI biomarkers in the clinical evaluation of antiangiogenic and vascular disrupting agents. *Br J Cancer*. 2007;96:189–195.
2. Taylor JS, Tofts PS, Port R, et al. MR imaging of tumor microcirculation: promise for the new millennium. *J Magn Reson Imaging*. 1999;10:903–907.
3. Ewing JR, Knight RA, Nagaraja TN, et al. Patlak plots of Gd-DTPA MRI data yield blood-brain transfer constants concordant with those of 14C-sucrose in areas of blood-brain opening. *Magn Reson Med*. 2003;50:283–292.
4. Zelhof B, Lowry M, Rodrigues G, et al. Description of magnetic resonance imaging-derived enhancement variables in pathologically confirmed prostate cancer and normal peripheral zone regions. *BJU Int*. 2009;104:621–627.
5. Alonzi R, Padhani AR, Allen C. Dynamic contrast enhanced MRI in prostate cancer. *Eur J Radiol*. 2007;63:335–350.
6. Kuhl CK, Mielcareck P, Klaschik S, et al. Dynamic breast MR imaging: are signal intensity time course data useful for differential diagnosis of enhancing lesions? *Radiology*. 1999;211:101–110.
7. Rieber A, Brambs HJ, Gabelmann A, et al. Breast MRI for monitoring response of primary breast cancer to neo-adjuvant chemotherapy. *Eur Radiol*. 2002;12:1711–1719.
8. Rouvière O, Raudrant A, Ecochard R, et al. Characterization of time-enhancement curves of benign and malignant prostate tissue at dynamic MR imaging. *Eur Radiol*. 2003;13:931–942.
9. Mayr NA, Yuh WT, Magnotta VA, et al. Tumor perfusion studies using fast magnetic resonance imaging technique in advanced cervical cancer: a new noninvasive predictive assay. *Int J Radiat Oncol Biol Phys*. 1996;36:623–633.
10. Zahra MA, Tan LT, Priest AN, et al. Semiquantitative and quantitative dynamic contrast-enhanced magnetic resonance imaging measurements predict radiation response in cervix cancer. *Int J Radiat Oncol Biol Phys*. 2009;74:766–773.
11. Akisik MF, Sandrasegaran K, Bu G, et al. Pancreatic cancer: utility of dynamic contrast-enhanced MR imaging in assessment of antiangiogenic therapy. *Radiology*. 2010;256:441–449.
12. Yankeelov TE, Gore JC. Dynamic Contrast Enhanced Magnetic Resonance Imaging in Oncology: Theory, Data Acquisition, Analysis, and Examples. *Curr Med Imaging Rev*. 2009;3:91–107.
13. Daniel BL, Yen YF, Glover GH, et al. Breast disease: dynamic spiral MR imaging. *Radiology*. 1998;209:499–509.
14. Mussurakis S, Gibbs P, Horsman A. Primary breast abnormalities: selective pixel sampling on dynamic gadolinium-enhanced MR images. *Radiology*. 1998;206:465–473.
15. Kumar AJ, Leeds NE, Fuller GN, et al. Malignant gliomas: MR imaging spectrum of radiation therapy- and chemotherapy-induced necrosis of the brain after treatment. *Radiology*. 2000;217:377–384.
16. Mullins ME, Barest GD, Schaefer PW, et al. Radiation necrosis versus. glioma recurrence: Conventional MR imaging clues to diagnosis. *Am J Neuroradiol*. 2005;26:1967–1972.
17. Rogers LR, Scarpace L, Guttierez J, et al. Magnetic resonance imaging characteristics and histological correlates of cerebral radiation necrosis. *Neurology*. 2006;66[Suppl 2]:335.
18. Jain R, Scarpace L, Ellika S, et al. First-pass perfusion computed tomography: initial experience in differentiating recurrent brain tumors from radiation effects and radiation necrosis. *Neurosurgery*. 2007;61:778–786.
19. Jain R, Narang J, Schultz L, et al. Permeability estimates in histopathology proven treatment induced necrosis using perfusion CT: Can these add to other perfusion parameters in differentiating from recurrent/progressive tumors? *AJNR Am J Neuroradiol*. 2011;32:658–663.
20. Sugahara T, Korogi Y, Tomiguchi S, et al. Post therapeutic intra axial brain tumor: the value of perfusion-sensitive contrast enhanced MR imaging for differentiating tumor recurrence from non neoplastic contrast-enhancing tissue. *AJNR Am J Neuroradiol*. 2000;21:901–909.
21. Barajas RF, Chang JS, Sneed PK, et al. Distinguishing recurrent intra-axial metastatic tumor from radiation necrosis following gamma knife radiosurgery using dynamic susceptibility-weighted contrast-enhanced perfusion MR imaging. *AJNR Am J Neuroradiol*. 2009;30:367–372.
22. Hein PA, Eskey CJ, Dunn JF, et al. Diffusion weighted imaging in the follow-up of treated high-grade gliomas: Tumor recurrence versus radiation injury. *Am J Neuroradiol*. 2004;25:201–209.
23. Kashimura H, Inoue T, Beppu T, et al. Diffusion tensor imaging for differentiation of recurrent brain tumor and radiation necrosis after radiotherapy—three case reports. *Clin Neurol Neurosurg*. 2007;109:106–110.
24. Rock JP, Scarpace L, Hearshen D, et al. Associations among magnetic resonance spectroscopy, apparent diffusion coefficients, and image-guided histopathology with special attention to radiation necrosis. *Neurosurgery*. 2004;54:1111–1117.
25. Cheronov M, Hayashi M, Izawa M, et al. Differentiation of the radiation induced necrosis and tumor recurrence after gamma knife radiosurgery for brain metastases: Importance of multivoxel proton MRS. *Minim Invasive Neurosurg*. 2005;48:228–234.

26. Graves EE, Nelson SJ, Vigneron DB, et al. Serial proton MR spectroscopic imaging of recurrent malignant gliomas after gamma knife radiosurgery. *Am J Neuroradiol*. 2001;22:613–624.
27. Rabinov JD, Lee PL, Barker FG, et al. In vivo 3-T MR spectroscopy in the distinction of recurrent glioma versus radiation effects: Initial experience. *Radiology*. 2002;225:871–879.
28. Chao ST, Suh JH, Raja S, et al. The sensitivity and specificity of FDG PET in distinguishing recurrent brain tumor from radionecrosis in patients treated with stereotactic radiosurgery. *Int J Cancer*. 2001;96:191–197.
29. Tsuyuguchi N, Sunada I, Iwai Y, et al. Methionine positron emission tomography of recurrent metastatic brain tumor and radiation necrosis after stereotactic radiosurgery: is a differential diagnosis possible? *J Neurosurg*. 2003;98:1056–1064.
30. Caravan P, Ellison JJ, McMurry TJ, et al. Gadolinium (III) chelates as MRI contrast agents: structure, dynamics and applications. *Chem Rev*. 1999;99:2293–2352.
31. Jain R, Narang J, Sundgren PM, et al. Treatment induced necrosis versus recurrent/progressing brain tumor: going beyond the boundaries of conventional morphologic imaging. *J Neurooncol*. 2010;100:17–29.
32. Lacerda S, Law M. Magnetic resonance perfusion and permeability imaging in brain tumors. *Neuroimaging Clin N Am*. 2009;19:527–557.
33. Buckley DL. Uncertainty in the analysis of tracer kinetics using dynamic contrast enhanced T1-weighted MRI. *Magn Reson Med*. 2002;47:601–606.
34. Choyke PL, Dwyer AJ, Knopp MV. Functional tumor imaging with dynamic contrast-enhanced magnetic resonance imaging. *J Magn Reson Imaging*. 2003;17:509–520.
35. Evelhoch JL. Key factors in the acquisition of contrast kinetic data for oncology. *J Magn Reson Imaging*. 1999;10:254–259.
36. Tofts PS, Brix G, Buckley DL, et al. Estimating kinetic parameters from dynamic contrast-enhanced T1-weighted MRI of diffusible tracer: standardized quantities and symbols. *J Magn Reson Imaging*. 1999;10:223–232.
37. Lee MC, Cha S, Chang SM, et al. Dynamic susceptibility contrast perfusion imaging of radiation effects in normal-appearing brain tissue: changes in the firstpass and recirculation phases. *J Magn Reson Imaging*. 2005;21:683–693.
38. Walker-Samuel S, Leach MO, Collins DJ. Evaluation of response to treatment using DCE-MRI: the relationship between initial area under the gadolinium curve (IAUGC) and quantitative pharmacokinetic analysis. *Phys Med Biol*. 2006;51:3593–3602.
39. Mills SJ, Soh C, O'Connor JP, et al. Enhancing fraction in glioma and its relationship to the tumoral vascular microenvironment: A dynamic contrast-enhanced MR imaging study. *AJNR Am J Neuroradiol*. 2010;31:726–731.
40. Roberts C, Issa B, Stone A, et al. Comparative study into the robustness of compartmental modeling and model-free analysis in DCE-MRI studies. *J Magn Reson Imaging*. 2006;23:554–563.
41. Evelhoch JL, LoRusso PM, He Z, et al. Magnetic resonance imaging measurements of the response of murine and human tumors to the vascular-targeting agent ZD6126. *Clin Cancer Res*. 2004;10:3650–3657.
42. Hazle JD, Jackson EF, Schomer DF, et al. Dynamic imaging of intracranial lesions using fast spin-echo imaging: differentiation of brain tumors and treatment effects. *J Magn Reson Imaging*. 1997;7:1084–1093.
43. Cha S, Lupo JM, Chen MH, et al. Differentiation of glioblastoma multiforme and single brain metastasis by peak height and percentage of signal intensity recovery derived from dynamic susceptibility-weighted contrast-enhanced perfusion MR imaging. *AJNR Am J Neuroradiol*. 2007;28(6):1078–1084.
44. Mitsuya K, Nakasu Y, Horiguchi S, et al. Perfusion weighted magnetic resonance imaging to distinguish the recurrence of metastatic brain tumors from radiation necrosis after stereotactic radiosurgery. *J Neurooncol*. 2010;99(1):81–88.
45. Hu LS, Baxter LC, Smith KA, et al. Relative cerebral blood volume values to differentiate high-grade glioma recurrence from posttreatment radiation effect: direct correlation between image-guided tissue histopathology and localized dynamic susceptibility-weighted contrast-enhanced perfusion MR imaging measurements. *AJNR Am J Neuroradiol*. 2009;30(3):552–558.
46. Barajas RF, Jr, Chang JS, Segal MR, et al. Differentiation of recurrent glioblastoma multiforme from radiation necrosis after external beam radiation therapy with dynamic susceptibility-weighted contrast-enhanced perfusion MR imaging. *Radiology* 2009;253(2):486–496.